2021-03-01

Diagnostics of a Large Volume Pin-to-Plate Atmospheric Plasma Source for the Study of Plasma Species Interactions with Cancer Cell Cultures

Laurence Scally
Technological University Dublin, BioPlasma Research Group, Dublin, Ireland

Chaitanya Sarangapani
Technological University Dublin

Brijesh Tiwari
Technological University Dublin

See next page for additional authors

Recommended Citation

Scally, L. et al. (2021) Diagnostics of a Large Volume Pin-to-Plate Atmospheric Plasma Source for the Study of Plasma Species Interactions with Cancer Cell Cultures,*Plasma Processes and Polymers,* e2000250 (2021) DOI:10.1002/ppap.202000250

Diagnostics of a Large Volume Pin-to-Plate Atmospheric Plasma Source for the Study of Plasma Species Interactions with Cancer Cell Cultures

Laurence Scally[1,5*], Sean Behan[1*], Andressa Maria Aguiar de Carvalho[1,2,6*], Chaitanya Sarangapani[1*], Brijesh Tiwari[2], Renee Malone[1], Hugh J. Byrne[3], James Curtin[1], and Patrick J. Cullen [4,5]

[1] BioPlasma Research Group, School of Food Science and Environmental Health, Technological University Dublin, City Campus, Dublin 1, Ireland.

[2] Department of Food Chemistry and Technology, Teagasc Food Research Centre, Ashtown, Dublin, Ireland.

[3] FOCAS Research Institute, Technological University Dublin, City Campus, Dublin 8, Ireland.

[4] University of Sydney, School of Chemical and Biomolecular Engineering, Sydney, Australia.

[5] PlasmaLeap Technologies, Dublin, Ireland.

[6] Environmental Sustainability & Health Institute (ESHI), Technological University Dublin, Dublin, Ireland.

* These authors contributed equally to this work.

Corresponding author: Laurence Scally (Laurence@plasmaleap.com)

Keywords: pin-to-plate, non-thermal plasma, optical spectroscopy, gas chemistry, plasma discharge frequency, reactive species, cell culture, glioblastoma multiforme.

Abstract

A large gap pin-to-plate, atmospheric pressure plasma reactor is demonstrated as means of *in vitro* study of plasma species interactions with cell cultures. By employing optical emission and optical absorption spectroscopy, we report that the pin-to-pate plasma array had an optimal discharge frequency for cell death of 1000 Hz in ambient air for the target cancer cell line; human glioblastoma multiform (U-251MG). The detected plasma chemistry contained reactive oxygen and nitrogen species including OH, N_2, N_2^+, and O_3. We show that, by varying the plasma discharge frequency, the plasma chemistry can be tailored to contain up to 8.85 times higher levels of reactive oxygen species as well as a factor increase of up to 2.86 for levels of reactive nitrogen species. At higher frequencies, reactive oxygen species are more dominant than reactive nitrogen species which allows for a more dynamic and controlled environment for sample study without modifying the inducer gas conditions. When used for treatment of culture media and cell cultures, variation of the plasma discharge frequency over the range 1000-2500 Hz demonstrated a clear dependence of the responses with the highest cytotoxic responses observed for 1000 Hz. We propose that the reactor offers a means of studying plasma-cell interactions and possible co-factors such as pro-drugs and nano particles for a large volume of samples and conditions due to the use of well plates.

1. Introduction

Studies of non-thermal plasma (NTP) have shown that they can be utilised for a wide range of applications, including; food preservation, wound sterilisation, enhanced crop growth, pollution abatement, volatile organic compound (VOC) removal, polymer functionalisation, and water purification.[1-5] Such a broad variability of applications is due to the large range of gas chemistries that can be generated using NTP systems. By using ambient air, reactive oxygen species (ROS) and reactive nitrogen species (RNS) can be generated to interact with target samples. Examples of ROS include O, O_2^*, O_3, OH, and NO, examples of RNS being N, N_2^*, N_2^+, and N_xO_y. These reactive species can interact with synthetic and/or biological samples and, when the plasma conditions are appropriately tailored, can cause alterations within cells that can lead to cancer cell death.[6] The plasma chemistry can be altered by introducing different gases into the system environment at varying percentages and ratios. For example, adding a small percentage of CO_2 into a system that is running predominantly on ambient air can lead to higher levels of O_3 formation, which can be further optimised with the introduction of other secondary gases such as Ar.[7-9] Introducing inert gases such as Ar and He gives rise to the production of inert excited species that can bombard and interact with sample surfaces and give rise to more binding sites or can aid in the formation of other reactive species, such as OH and N_2^*, through synergistic energy transfers.[10]

An emerging research focus in the applications of plasma science is the treatment of cancer cells to develop alternatives or complementary treatments to conventional therapeutic approaches.[11] Interest in the use of NTP sources for cancer treatment has arisen due to their ease of use, the potential for minimising treatment side effects, and reducing damage to healthy cells by more specifically targeting cancerous cells. This potential comes from the versatile chemistry produced by NTP discharges. Numerous *in vitro* studies have shown that cytotoxicity can be induced through the generation of RONS, causing a disruption of various

cell functions.[12, 13] Claims as to which reactive species are responsible for cancer cell death identify H_2O_2, OH, O_2^-, O_3 and NO_x as important candidates.[12, 13] There are a host of possible chemical reactions and pathways that occur within plasma discharges and the sample boundaries to which they are exposed, but some samples are more resilient to particular reactive species, while being susceptible to others. Specific assays can be carried out to determine which species and reaction pathways are most likely to induce cytotoxicity in cancer cells. Through different comparative methods, studies have shown that the presence of ROS, such as peroxides and superoxides, causes intracellular stress to a greater extent than RNS, for *in vitro* treatments of various human cell lines, including glioblastomas, brain, lung, blood, cervical, melanoma, and breast cancer.[12, 14] The use of NTP discharges can be employed to disrupt the growth of various cancer cells, with lower cytotoxic impact on normal host cells, due to preferential ROS interactions that can initiate cell cycle disruption and apoptosis in cancerous cells.[15, 16]

Given that the gas chemistry interactions of the plasma discharge are the most important factors in plasma processing techniques, there are many variables that need to be considered in order to optimise NTP systems for specific applications. These include voltage, discharge frequency, duty cycle, discharge gap, electrode geometry, and dielectric material selection. It is well known that varied input power to a system (voltage, current, and pulse) gives rise to more intense, and possibly differing modes of plasma discharges.[17] Recently, focus on electrode designs has allowed NTP systems to become much more versatile, efficient, and to create more homogeneous discharges for more equal surface interactions.[18-22] One of the designs that has been developed and investigated is pin-to-plate based electrodes. By creating an array of pins that are connected to a high voltage source and allowing a plate electrode to act as the ground, a stable and efficient plasma can be achieved.[23] The efficiency can be seen in the relatively lower values of power consumption compared to purely plate-to-plate dielectric barrier discharge systems, resulting in a more diffusive nature of the discharge over

sample surfaces.[23, 24] Utilising pin type electrodes can enable finer control over the distribution of the electric field, which leads to a focusing effect that produces a more energetic and dense plasma. This can then result in a higher number of streamer channels which form higher levels of reactive species due to higher gas collision and excitation rates. It has also been shown that each pin within such pin-to-plate systems creates a diffusive discharge that has an area much larger than the area of the pin tip.[23] These qualities create an environment that allows for more interactions between reactive species and samples being treated, thus enabling better coverage of sample surface areas, speeding up treatment processes, and aiding in larger scale plasma discharges to be generated.

In the current work, a novel pin-to-plate NTP system is characterised, and the dependence of its efficacy for cell death on plasma generation conditions is demonstrated in a human cancer cell line U-251MG, cultured *in vitro*. In order to gain more insight into the interactions of non-thermal plasma discharges and how they create an environment conducive to higher levels of reaction mechanisms, the plasma discharge is initially characterised and optimised by a combination of optical absorption spectroscopy (OAS) and optical emission spectroscopy (OES). The effect of the plasma discharge conditions on the generation of reactive species in cell culture medium is then investigated. Finally, it is demonstrated that optimised plasma discharge conditions can lead to enhanced cell death rates in human cancer cells, *in vitro*.

2. Materials and Methods

2.1 System Configuration

A large gap pin-to-plate electrode was employed, which facilitated the insertion of well plates into the plasma discharge. The 88-pin stainless-steel electrode was supplied by PlasmaLeap Technologies (Dublin, Ireland). The ground and HV electrodes were made of stainless steel with a discharge gap of 4 cm between them. The gap between each pin was 14 mm with the dimensions of the pins being: length of 25 – 29 mm and diameter 2 mm. In order to create a plasma discharge that is as homogeneous as possible throughout the discharge volume, the pins are arranged in a slightly convex manner. This is done by varying the length of the pins on the stainless-steel high voltage plate such that they are gradually set closer to the stainless-steel ground plate from the edge of the pin array to the centre, leaving the central pins the closest to the ground plate. By using this geometry, the electric field is distributed to minimise the losses at the edge and corners of the high voltage plate. The electrode configuration was powered by an AC supply (Leap100, PlasmaLeap Technologies, Dublin, Ireland). The design facilitated the control of resonance frequency (30-125 kHz), discharge frequency (50 – 3000 Hz), power (50 – 400 W), with a discharge gap of a maximum of 55 mm. For this study, the duty cycle was set at 54, 72, or 90 μs. The resonant frequency was set at 55.51 kHz, and the discharge frequency was varied in the range 100 – 2500 Hz. The discharge gap was kept at 40 mm, the samples prepped for treatment being placed in the centre of the system on the ground plate. Figure 1 shows how the system was set up for sample treatment.

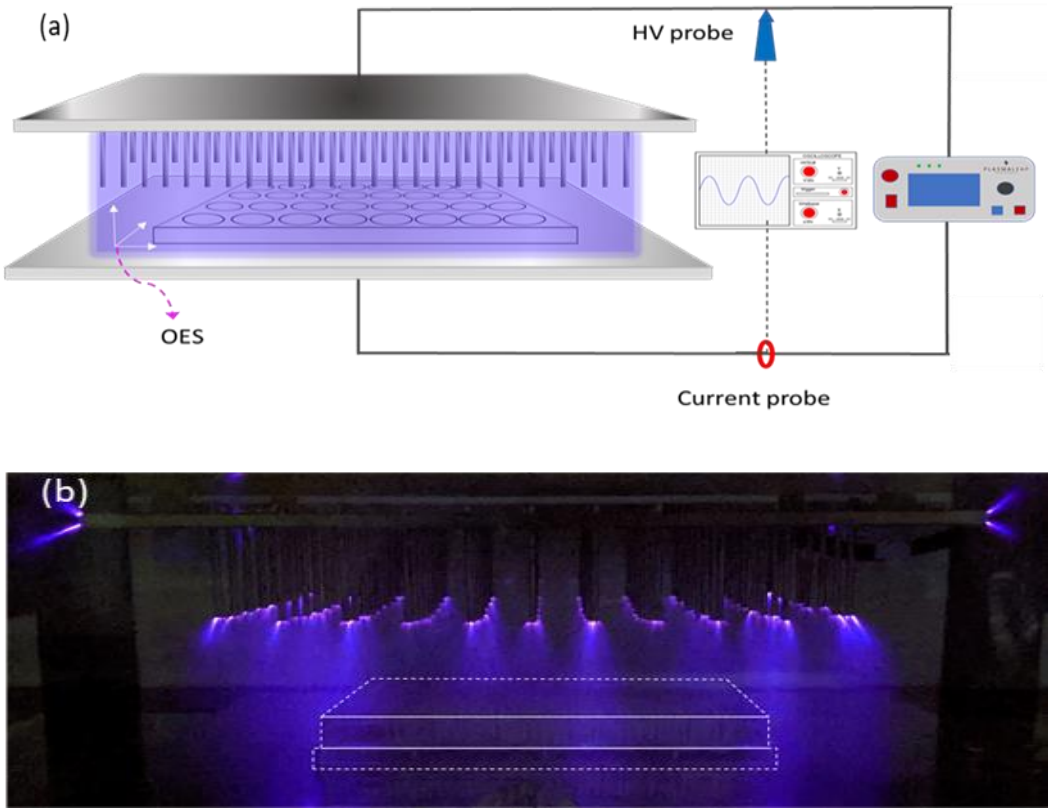

Figure 1: Schematic and photograph of the pin reactor, with the inclusion of a well plate in the discharge gap. (a) Schematic of the pin reactor used (b) Photograph of the atmospheric air discharge.

2.2 Electrical Characterisation

The electrical characterisation of the system was performed by connecting a passive probe (CP6990-NA Cal Test Electronics, Yorba Linda, CA, USA) to the ground wire in order to measure the current and by having a high voltage probe (VD-100 North Star, Bainbridge Island, WA, USA) connected in parallel to the high voltage and ground plate to measure the applied voltage. By measuring the output voltage and current from the transformer, the power needed

to generate the plasma discharge can be measured and maintained for continuous use and better repeatability. Current measurements can also be used to ascertain the behaviour of the plasma discharge as the fluctuation in current represents changes in electron energetics.

2.3 Optical Diagnostics

2.3.1 OES

In order to determine the gas chemistry of the plasma discharge and the interactions that may occur at the sample boundary of the cell culture media during treatment, OES and OAS were used to monitor and characterise the reactive species formed in the discharge. Both of these measurement techniques were carried out by using an Edmund Optics CCD spectrometer that has a wavelength range of 200 – 850 nm. To record the spectra during the measurement processes, for both OES and OAS, the software BWSpec^{TM} was used. The spectral resolution for this particular spectrometer is between 0.6 and 1.8 nm and is wavelength dependent. Due to the limited spectral resolution, there may be overlap of emission lines of certain species, which leads to a need for a deconvolution process. However, in this study, the spectral lines that are studied are separated by large enough ranges that the peaks of interest have no overlap with those of other emissive species. OES measurements were carried out at 15 points on the NTP system used in this study. The first point was set at a (0, 0) coordinate at the ground plate, below where the first row of pins began, and the subsequent points were set at 4 cm intervals up to 16 cm to the right of the initial position. These were set at 2 cm and 4 cm above the ground plate to give a full spatial interpretation of the plasma discharge. The acquisition of each spectrum was carried out with an integration time of 2000 ms and the time between each spectrum was 5.5 s. In order to carry out these measurements, a fibre optic cable was used that had an adjustable lens attached to the end and was directed perpendicular to the system. The species that were detected with OES were OH at 300 nm, N_2 from the second positive system

(SPS) from 315-380 nm, and N_2^+ from the first negative system (FNS) at 391 nm. After finishing the OES measurements, the spectra were analysed by integrating the area under each peak of interest to calculate the value of the total intensity, in arbitrary units.

From the OES data obtained, a line ratio method was used to determine the distribution of electron energies within the discharge.[10] Given that the spectrometer used gives the intensity results in arbitrary units, the method employed only gives an indication as to whether there is a higher density of low or high energy electrons. From this, the most probable reaction mechanisms and how certain species are formed can be asserted. By using the total emission intensity of N_2 at 337 nm and the total emission intensity of N_2^+ at 391 nm, the line ratio shown in equation 1 can be used. It has been demonstrated in other works that the dominant route for the excitation of these two species is from direct electron excitation.[25, 26] The excitation energy of N_2 at 337 nm is 11.01 eV and the excitation for N_2^+ at 391 nm is 18.8 eV. From this, the line ratio gives a good indicator as to the electron energy distribution function (EEDF) and what energetics can be expected within the plasma discharge with respect to the spatial and temporal evolution of the gas chemistry.

$$EEDF = \frac{I(337\ \text{nm})}{I(391\ nm)} = \frac{I(N_2)}{I(N_2^+)} \quad (1)$$

2.3.2 OAS

With regard to OAS measurements, there may be an overlap of different light absorbing reactive species, as there can be a large band of absorbed wavelengths with a resonant absorption wavelength. Of interest in this study was O_3, which has a strong absorbance in the UV-region of the spectrum. There are, however, other reactive species that may absorb in this region, such as NO_2. In order to determine whether or not there would be any influence and

interference from this, Dräger tubes were used to detect whether there was any concentration of NO_2 after plasma discharge. From this, there was found to be no detectable amounts of NO_2 and the emission spectrum in Figure 4(d) shows no detectable amounts of NO that are typically found between 240 – 260 nm. The gas chemistry that has been measured, and that is explained in greater detail in section 3, gives an insight into the reaction mechanisms giving rise to the generation of reactive species. On this basis, the evaluation of O_3 became the main objective of the OAS measurements.

In order to carry out the OAS measurement of the generated plasma, two fibre optic cables were used. Both had adjustable lenses to optimise the focal point of detection. They were placed perpendicular to one another at a distance of 25 cm and had a direct line-of-sight between them. One fibre optic cable was connected to a deuterium-tungsten UV-Vis-NIR light source and the other to the CCD spectrometer to detect the incoming light. By referencing the incoming light from the plasma discharge, the average optical density of different absorbing species can be determined. The spectra were measured with an integration time of 550 ms at intervals of 1450 ms between each measurement. OAS measurements were analysed using equation 2 to find the average spatial density of O_3 during the plasma discharge and post-discharge. In equation 2, *D(t)* is the average spatial density (cm^{-3}), *L* is the optical path (cm), *I(0)* is the reference intensity with no plasma discharge (A.U.), *I(t)* is the measured intensity (A.U.) during and after plasma discharge, and $\sigma(\lambda)$ is the wavelength dependent absorption cross-section for the species of interest. For O_3, the wavelength of optimal absorption is taken as 253.7 nm which gives an absorption cross-section value of 1.154 x 10^{-17} cm^2.[8]

$$D(t) = \frac{1}{\sigma(\lambda)L} ln \frac{I(0)}{I(t)} \quad (2)$$

2.4 Chemical Analysis of Reactive Species in cell culture medium

Nitrite concentrations in the plasma treated water and Dulbecco's modified eagle's cell culture medium (DMEM) samples were quantified by employing the Griess reagent (N-(1-naphthyl) ethylenediamine dihydrochloride) spectrophotometric method.[27] This was accomplished by the addition of 100 µl sample, trichloroacetic acid and Griess reagent. The reaction mixture was incubated at 37 °C for 30 min, after which the absorbance was determined at a wavelength of 548 nm using a UV–visible spectrophotometer (Shimadzu UV-1800, Shimadzu Scientific Instruments Kyoto, Japan). A calibration curve was prepared using a standard solution of sodium nitrite. Nitrate concentrations were determined according to the procedure in reference [27]. Hydrogen peroxide concentrations were determined using the titanium oxysulfate colorimetric method.[28] For this purpose, a total of 10 µl $TiOSO_4$ solution were added to 100 µl of treated samples. After 10 min incubation, with the same conditions previously used, absorbance was read on a spectrophotometric plate reader at a wavelength of 405 nm.

2.5 Cancer Cells Cytotoxicity

2.5.1 Cell Culture

Human glioblastoma multiform (U-251MG, formerly known as U-373 MG-CD14) cells were obtained from Trinity College Dublin, Ireland. Human epithelial carcinoma (A431) cells were purchased from ATCC European Distributor (LGC Standards, Teddington, UK). Cells were cultivated with DMEM - Dulbecco's Modified Eagle Medium without sodium pyruvate (Sigma-Aldrich, Merck Group, Arklow, Ireland) and supplied with 10% FBS (Sigma-Aldrich)

and 1% penicillin/streptomycin (Sigma-Aldrich). U251MG cells were maintained in a humidified incubator containing 5% CO_2 at 37 °C.

2.5.2 Cell viability assay

U251MG cells were seeded at a density of 2 x 10^3 into flat bottom 96 well-plates (Sarstedt, Ltd., Wexford, Ireland) and allowed to adhere overnight. 80 µL of medium were removed before treatment, leaving 20 µL of medium in each well. In order to determine the optimal discharge frequency for sample treatments, the cytotoxic effects of the pin-to-plate device on U251MG human multiforme glioblastoma cells were measured at discharge frequencies of 1000, 2000, and 2500 Hz at 240 V and 72 µs. Plates were then treated with the pin-to-plate discharge at 7 different time points (5, 10, 20, 40, 80, 160, 320 – (s)) using a duty cycle of 72 µs, 240 V and frequency of 1000 Hz. Fresh medium was added to the wells after treatment and cells were then incubated at 37 ºC for 96 hours.

Cell viability was analysed using the Alamar Blue™ Cell Viability Reagent (Thermo Fisher, Dublin, Ireland), a resazurin-based solution that functions as a cell viability indicator by using the reducing power of living cells to quantitatively measure viability.[29] Cells were washed once with phosphate-buffered saline (PBS) and incubated for 3 hours at 37 °C with a 10% Alamar Blue™ solution. Fluorescence was measured using an excitation wavelength of 530 nm and an emission wavelength of 595 nm on a Varioskan Lux multi-plate reader (Thermo Fisher). All experiments were performed at least three independent times with a minimum of 24 replicates per experiment. Cytotoxicity data was fitted to determine the Inhibitory Concentration (IC_{50}) using a 4 parameter Hill equation of the form $f(x) = min + (max-min)/(1+(x/IC_{50})^{n})$, where n is the Hill slope.

3. Results and Discussion

A combination of electrical and optical measurements were employed to identify the optimum operating parameters for reactive species generation. Following optimisation of the parameters, these were then used for the treatment of U251MG human glioblastoma multiforme cells.

3.1 Electrical Characterisation

Varying the voltage, duty cycle, and discharge frequency and measuring the changes in the actual current and voltage across the system in response to parameter changes provided insights into the dynamics that occur within the discharge.

The discharge frequency was initially varied to determine which frequency was optimal for generating the plasma discharge. Figure 2(a) shows that, between 100 – 3000 Hz, the discharge voltage increases and reaches a plateau at 600 Hz, at which point it begins to steadily decline. Figure 2(b) highlights changes in the current measured with respect to the discharge frequency. Overall, the current decreases significantly, but plateaus in the range from 100 – 500 Hz and from 2000 – 2600 Hz. Overall, the system maintains a plasma discharge characterised as a glow discharge. The effects observed can be explained by the interaction of the electric field and the impact it has on electron excitation and, therefore, plasma ignition. Both the low and high discharge frequencies induce instabilities and cause premature quenching of the plasma. When the discharge frequency is too low for the system being used, electrons accumulate rapidly and cause the opposing electric field to increase too quickly and suppress the rise of the applied voltage. For this system, the lower frequency range is prescribed as being 0 – 800 Hz. On the other hand, when the discharge frequency is too high, the electrons that are formed in the plasma bulk become trapped within the inner electrode space and are unable to reach the electrodes to form the opposing electric field. For this system, the lower frequency range is prescribed as being 1900 – 3000 Hz. Both events prematurely quench the

plasma discharge.[31] Therefore, the discharge frequency must allow for electron kinetics to reach a high enough energy to create a strong plasma discharge that has a higher level of electron kinetics, but not so much that they induce a self-quenching event. The optimum discharge frequency for this work was found to be 1000 Hz, which was further validated by the optical results shown in Figures 4 and 5.

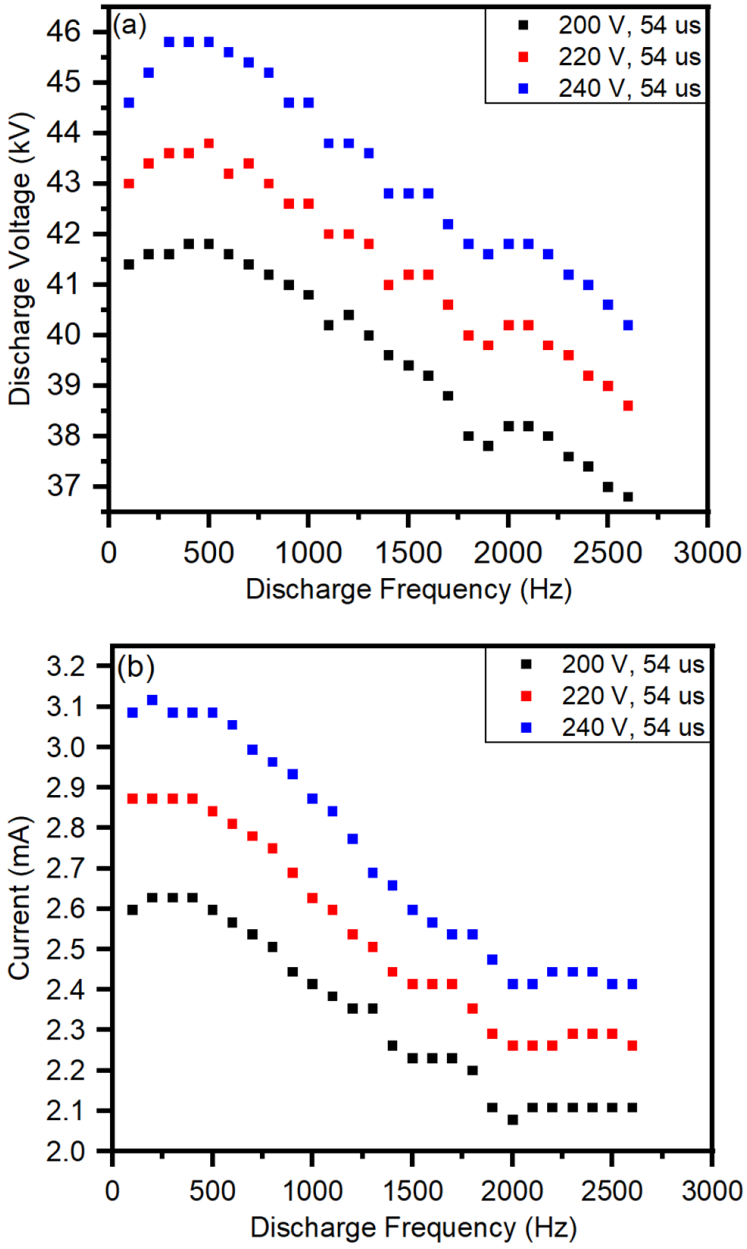

Figure 2: (a) the changes in discharge voltage with frequency and (b) the change in current with respect to frequency. For each graph, the duty cycle was kept at 54 µs.

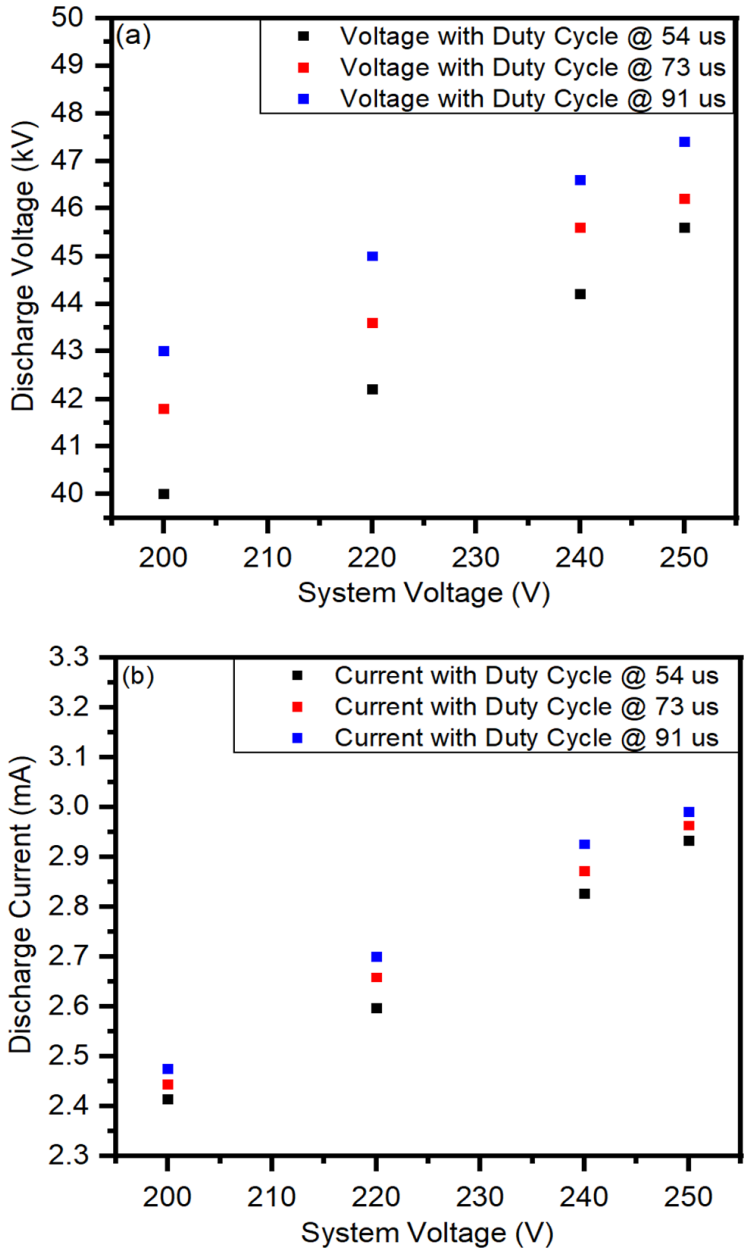

Figure 3: (a) changes in discharge voltage with variation in system voltage and duty cycle and (b) the change in current with variation in system voltage and duty cycle. For each of these graphs, the discharge frequency was kept at 1000 Hz.

3.2 Optical Diagnostics

3.2.1 Parameter Optimisation

OES and OAS were used to measure the formation of different reactive species over time as a function of voltage, duty cycle, and discharge frequency. As can be seen in Figure 4(a), the optimum discharge frequency for the formation of N_2 at 337 nm, and by association of the SPS group, given the similar excitation energies, is 1000 Hz. Although there are comparable levels detected at 1300 Hz, there is a larger fluctuation over the timescale of the measurement (1-70 sec). In Figure 4(b), it can be seen that the largest formation of N_2^+ occurs at the lower frequencies (600 and 800 Hz) and at 1300 Hz. The higher levels of N_2^+ detected at the lower frequencies is due to the higher energetics of the electrons. Although not quite self-quenching at this point, there is still an issue of initiating a large cascade event to form more reactive species, and so the kinetic transfer of energy through collisional means excites N_2 to N_2^+. This is evident when noting that low levels of excited N_2 at 337 nm are seen at these lower frequencies. However, there is a relatively large amount of N_2^+ generated at 1000 Hz. Given that there is a higher and consistent level of N_2 from 337 nm (and the SPS) at 1000 Hz and a relatively high level of N_2^+ formed at the same discharge frequency, it seems optimal to use this value for cell target study.

OAS data can be employed to support the evidence that 1000 Hz is the optimum discharge frequency. As can be seen in Figure 5, the average spatial density of O_3 increases with the plasma discharge time. It is also observed that the lifetime of O_3 is considerable and there is a substantial density remaining within the discharge zone when the plasma discharge has ceased. This allows for the option of leaving samples within the system for a period post discharge. Although there is a range of frequencies within which the highest amount of O_3 is

formed, the optimum is again suggested to be 1000 Hz, as this allows for an equally high generation of N_2 and N_2^+.

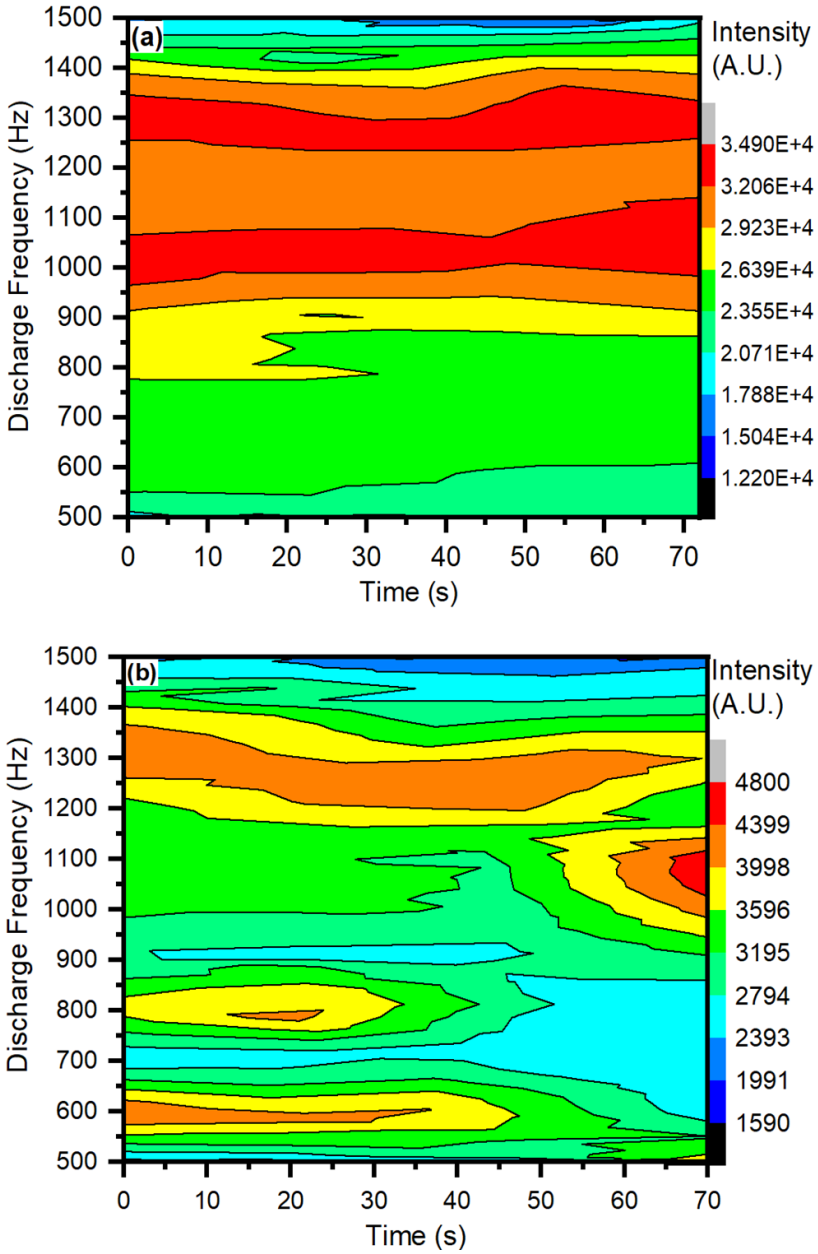

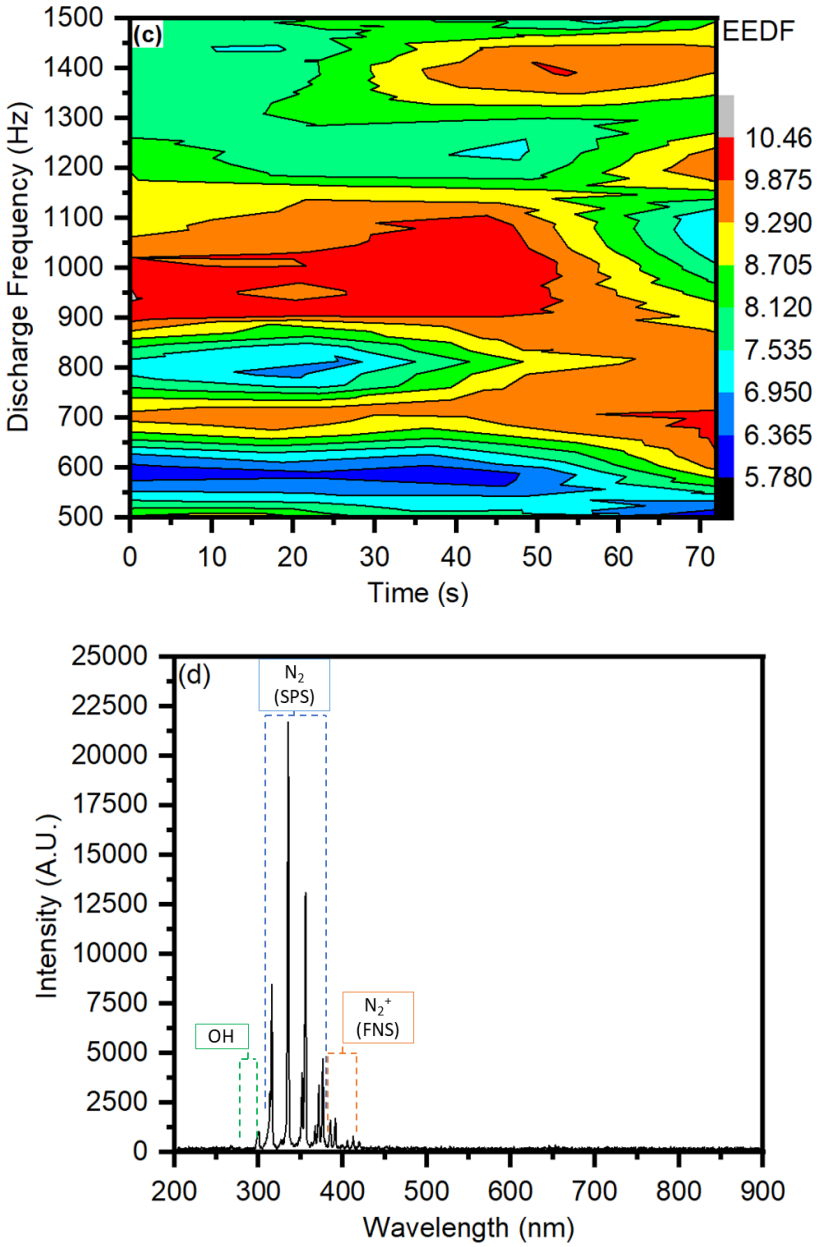

Figure 4: Changes seen in (a) N_2-337 nm (b) N_2^+-391 nm and (c) the EEDF calculated from the line ratio of (337 nm/391 nm) (d) single spectrum of all detected emission species.

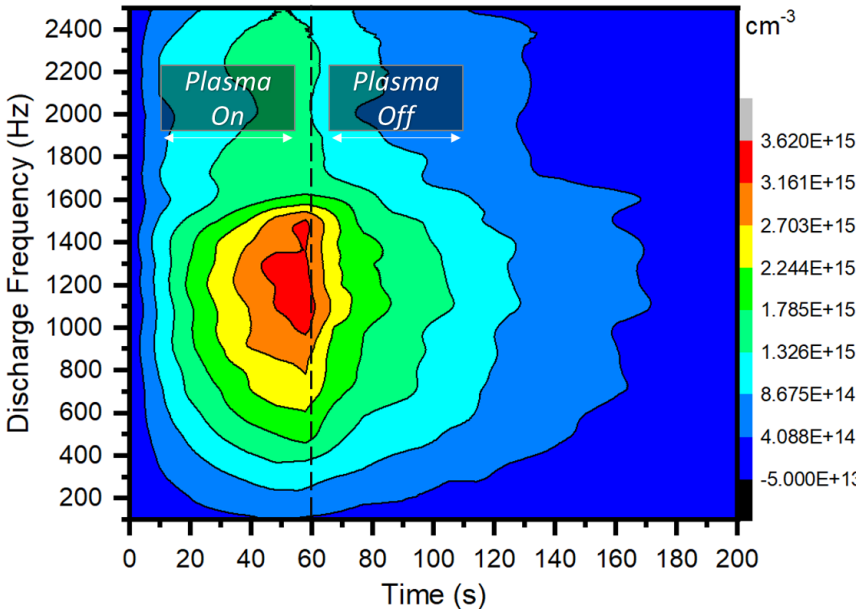

Figure 5: The variation of the average spatial density of O_3 with respect to the discharge frequency and temporal evolution. The plasma discharge was set to run for 60 s and the total measurement time was 200 s. This was to allow for measurement of O_3 during and post-discharge.

3.2.2 Spatial Characterisation

The spatial evolution of the total intensity of N_2 from the SPS is shown in Figure 6(a). This was measured by investigating each peak found in this group, being 315, 337, 357, and 380 nm. Each was found to follow the same trend as shown for N_2-337nm in Figure 4(a). The maximum values were found to be at the tip of the edge pins, where the electric field is highest. and where the border of the discharge zone meets the surrounding ambient air. Greater levels of N_2 are expected to be formed at the boundary, as there is lower quenching as a result of reduced reaction rates due to the electronegativity of other reactive species (i.e. O_3). The intensity of N_2^+, the only emission detected that belongs to the FNS, is shown in Figure 6(b). It follows a similar trend to that seen for N_2 of the SPS and the same reasoning can be applied. Figure 6(c) shows that the OH values are highest around the pin region and are relatively

consistent throughout the rest of the discharge volume. This may be due to the interactions that occur between O, O_2, O_3, and H_2O. Although there is no detection of atomic oxygen, it is reasonable to assume that the majority are converted to O_3. What remains from these reactions may still be in a sufficiently energetic state to dissociate H_2O due to its low excitation levels and give rise to the formation of more OH, as shown in equations 1-3, in which *M* is a third chemical constituent. In ambient air, *M* may be N_2^*, O, NO, NO_2, or OH. Figure 6(d) shows the EEDF of the system using the line ratio of (N_2-337 nm/N_2^+-391 nm) and highlights that the central locations are dominated by lower energy species when compared to N_2^+. These include N_2(SPS) and OH, which have excitation energies of 11 eV and 4.17 eV, respectively. This could be due to the quenching of N_2^+ in the interactions and mechanisms that form O_3, reducing the amount of detected emissions from this energetic species, due to loss of energy through more collisional processes.

$$O_2 + e_{fast} \rightarrow O^* + O^* + e_{slow} \quad (1)$$

$$O^* + H_2O \leftrightarrow 2OH \quad (2)$$

$$O^* + O_2 + M^* \rightarrow O_3 + M \quad (3)$$

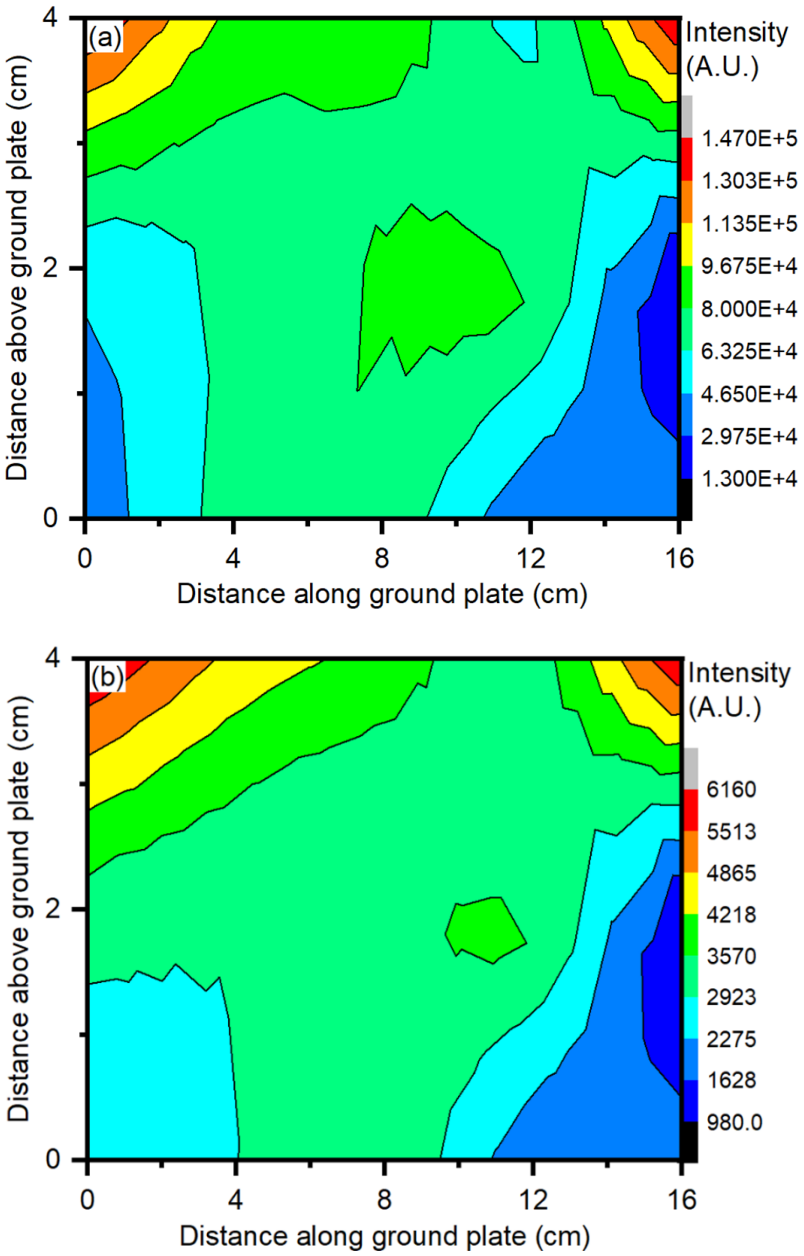
(a)
Intensity
(A.U.)
1.470E+5
1.303E+5
1.135E+5
9.675E+4
8.000E+4
6.325E+4
4.650E+4
2.975E+4
1.300E+4
Distance above ground plate (cm)
Distance along ground plate (cm)
0
2
4
0
4
8
12
16
(b)
Intensity
(A.U.)
6160
5513
4865
4218
3570
2923
2275
1628
980.0
Distance above ground plate (cm)
Distance along ground plate (cm)

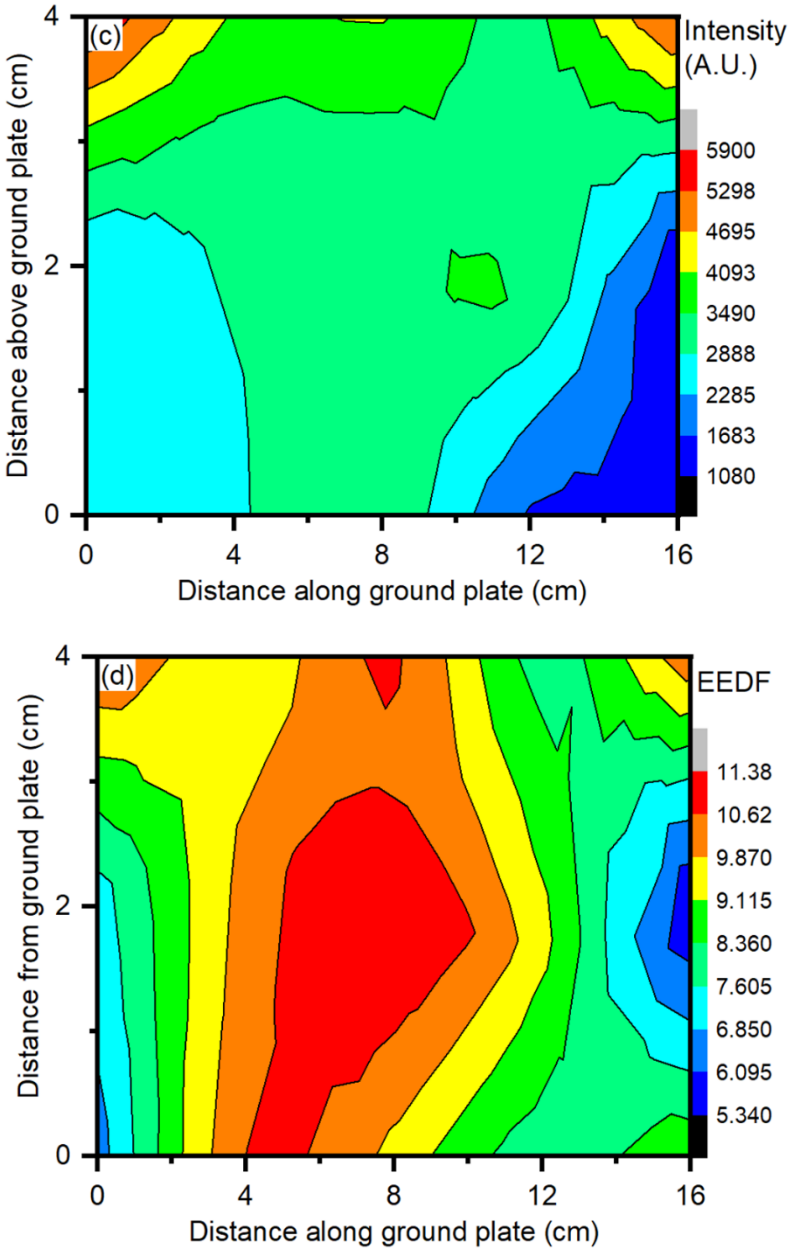

Figure 6: OES measurements that show the spatial evolution of the emission species that were detected in this experiment and are (a) total intensity from the SPS (b) intensity of N_2^+ at 391 nm (c) intensity of OH measured at 300 nm and (d) the EEDF from the line ratio of (391nm/337nm) based on the values from (a) and (b).

Figure 7 shows the spatial evolution of O_3 and its average spatial density. It is shown that the highest values of O_3 are along the pin tips and throughout the central portion of the system, towards the ground plate. The likely reasons for this are twofold. Firstly, the edge of

the system has high fluctuations of O_3, as it is at the boundary edge of the system, and the direct electric field. This gives less time for the reactive species to dwell within the electric field and maintain high energetic levels, and any O_3 generated is readily dissociated through collisional processes with other atomic and molecular species, transferring its gained energy in the resulting kinetics. Secondly, the central part of the system will most likely have a better electric field distribution, exciting species to higher levels and allowing them to maintain such energetic states by allowing them to have a longer residence time in the direct electric field.

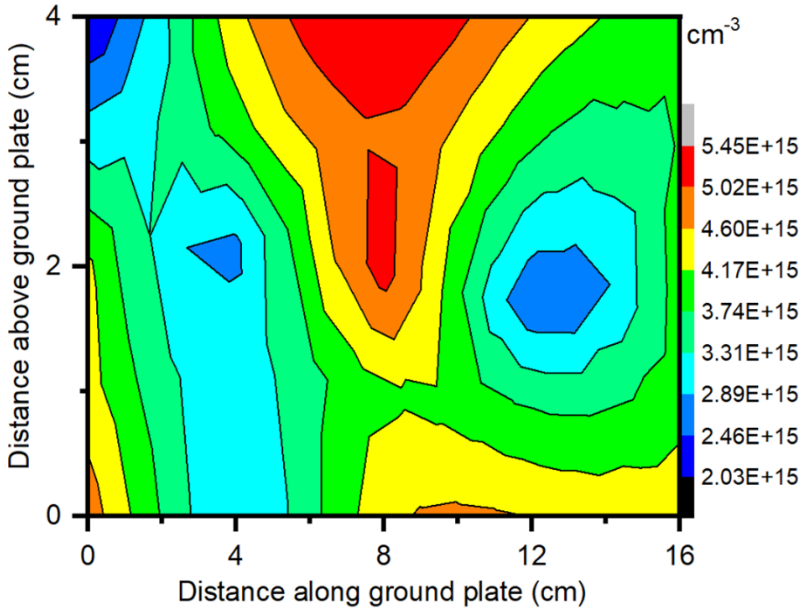

Figure 7: Spatial evolution of O_3 using the maximum value found after 300 s of discharge with the voltage set at 240 V and the duty cycle at 91 µs.

3.3 Reactive Species Formation in Liquids

The analysis of section 3.2.1 suggests that the characteristics of the plasma discharge are dependent on the discharge frequency, and that the optimal operation frequency is ~1000 Hz. In terms of applications for treatment of cell cultures, the performance optimisation was therefore checked by monitoring the effects of the treatment on cell culture medium, by monitoring the production of several metastable species, namely nitrite, nitrate, and hydrogen

peroxide in both deionised (DI) water and DMEM cell culture medium. This was carried out as a function of discharge frequency at a fixed time of 5 minutes and as a function of time at a fixed frequency of 1000 Hz. Figure 8 shows that the values of all species were highest at 1000 Hz. Figure 9(a) indicates that this concentration increases monotonically over the exposure time of 0 – 320 seconds. For the case of nitrate species, the measurement similarly shows a maximum measured value at 1000 Hz, and an evolution which is continuing to increase after 320 sec exposure, as shown in Figure 9(b). A similar trend is shown for H_2O_2 generation. However, it can be seen that the production rate is maximum at the early stages of exposure and begins to saturate after 1-2 minutes. The results of the analysis further confirm the importance of discharge frequency for applications such as the treatment of biological samples.

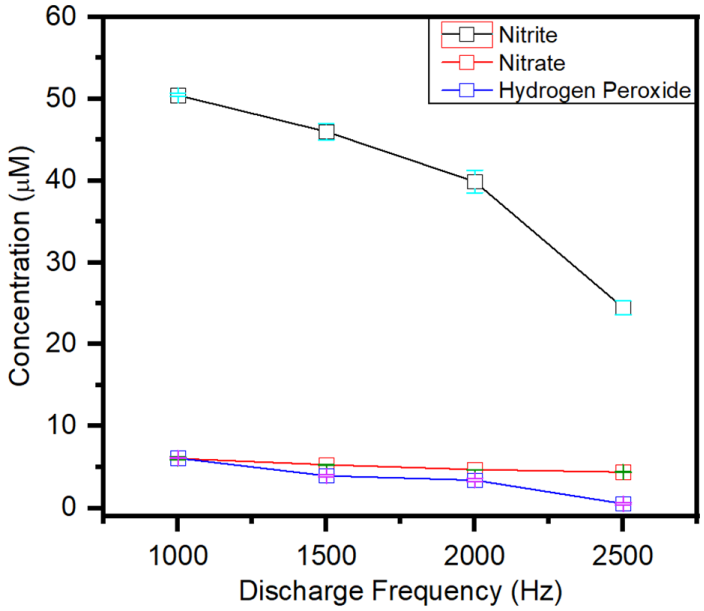

Figure 8: Concentration values of the reactive species measured within DMEM after 5 minutes of treatment at 240 V and 74 μs shows an optimisation of the plasma discharge at 1000 Hz.

The reactive species generated during plasma treatment undergo several chemical reactions to form ROS, such as OH and H_2O_2. The concentrations of H_2O_2 were seen to increase gradually with increased treatment time, up to ~140 uM after 320 s treatment, in both deionised

water and DMEM. Due to their short lifetime (3.7×10^{-9}s), OH radicals diffusing from the plasma zone to the liquid interface undergo recombination to form hydrogen peroxide (oxidation potential 1.77 V).[31] Hydrogen peroxide in the sample solutions can be directly or indirectly generated via various reaction mechanisms (e.g., dissociation, photolysis), as described by Equations 4-8.

$$O_3 + OH \rightarrow HO_2 + O_2 \quad (4)$$

$$OH + OH \rightarrow H_2O_2 \quad (5)$$

$$O_2 + H \rightarrow HO_2 \quad (6)$$

$$H + HO_2 \rightarrow H_2O_2 \quad (7)$$

$$H_2O_2 + O_3 \rightarrow OH + O_2 + HO_2 \quad (8)$$

As can be observed in Figure 9, there is an increase in the concentration of nitrates and nitrites in both deionised water and DMEM, which can significantly change both the fluid pH and electrical conductivity. The dissolution of nitrate to form nitric acid can be explained by reaction mechanisms 9 to 14. During plasma treatment, the production of NO mainly follows the Zeldovich mechanism.[31] The NO formed can be oxidised to NO_2. NO and NO_2 can subsequently dissolve in water to form nitrates and nitrites (HNO_3, NO_3, and NO_2).[27] Given that there was no emission detected for NO and there were no levels of NO_2 detected using Dräger detection tubes, they either form and interact immediately with other species and have their lifetime reduced or are generated predominantly at the plasma-media boundary. From the concentrations measured, the reaction pathways that generate H_2O_2 may be the most dominant interactions at the boundary. Reaction mechanisms 15 - 16 are then suggested as possible pathways.

$$N_2 + e \rightarrow 2N + e \quad (9)$$

$$N + 2O \rightarrow NO_2 \quad (10)$$

$$NO_2 + H_2O_2 + H_3O \rightarrow HNO_3 + 2H_2O \quad (11)$$

$$HNO_3 + 2H_2O \rightarrow NO_3 + H_3O \quad (12)$$

$$NO_2 + OH \rightarrow HNO_3 \quad (13)$$

$$N_2 + O_3 + OH \rightarrow HNO_3 + NO \quad (14)$$

$$HNO_3 + OH \rightarrow H_2O_2 + NO_2 \quad (15)$$

$$HNO_3 + O_2 \rightarrow H_2O_2 + NO_3 \quad (16)$$

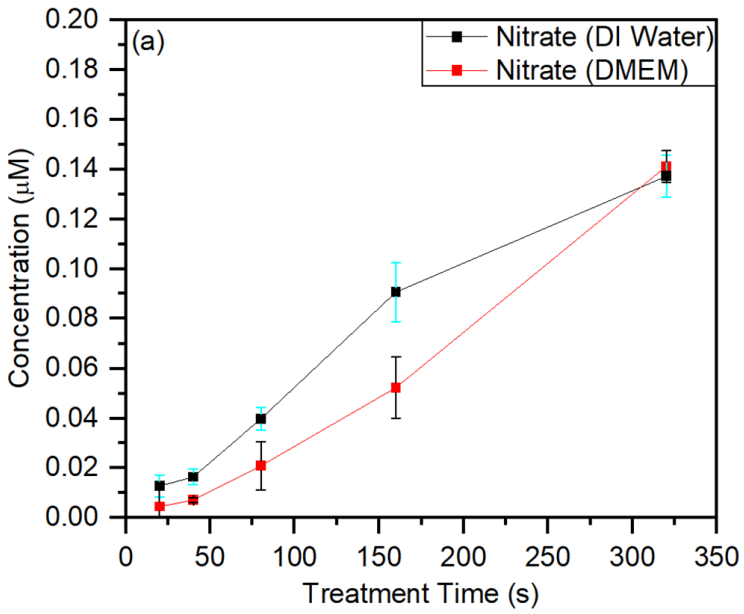

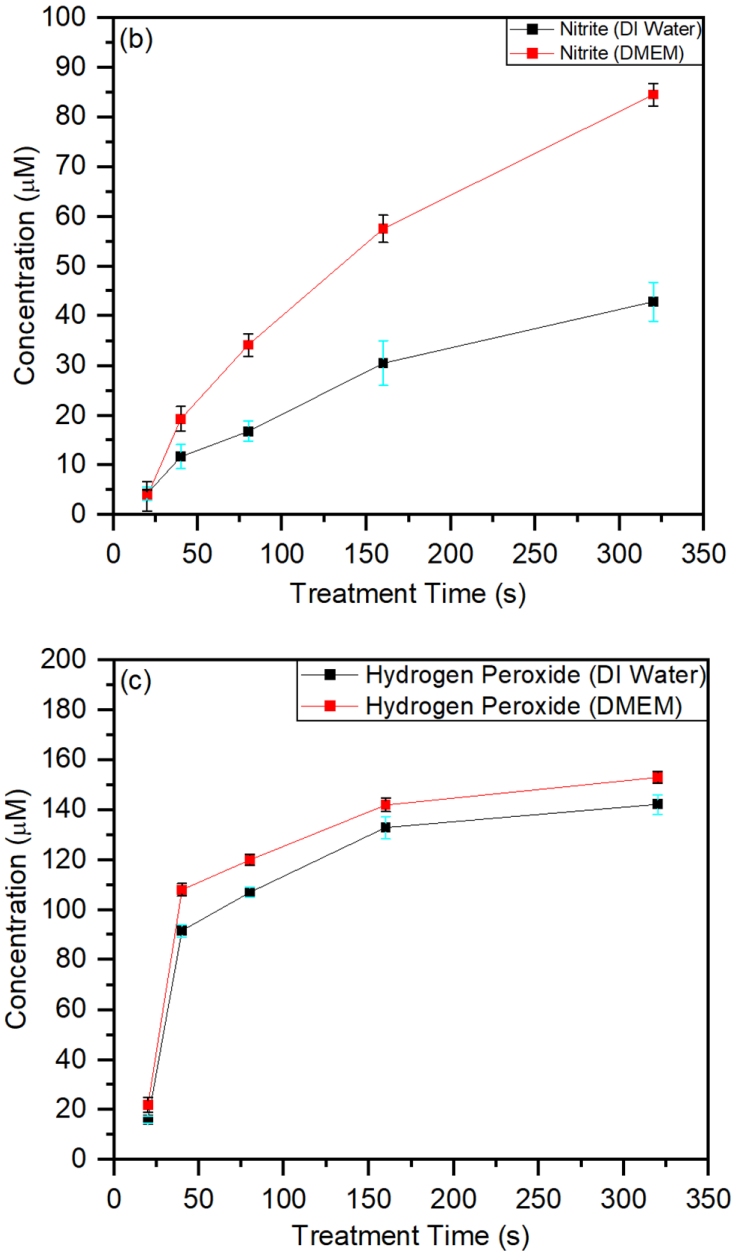

Figure 9: Changes in the formation of reactive oxygen and reactive nitrogen species over time in deionised water and DMEM with settings at 240 V, 74 µs, and 1000 Hz

3.4 Cytotoxicity

From the optical plasma diagnostics data and chemical analyses of plasma treated DI water and DMEM, the optimal frequency for generating the gas chemistry with the highest concentration of both ROS and RNS is 1000 Hz. Varying the voltage and duty cycle can be shown to significantly affect the levels, but, comparably, the discharge frequency has the largest impact for plasma discharge optimisation.

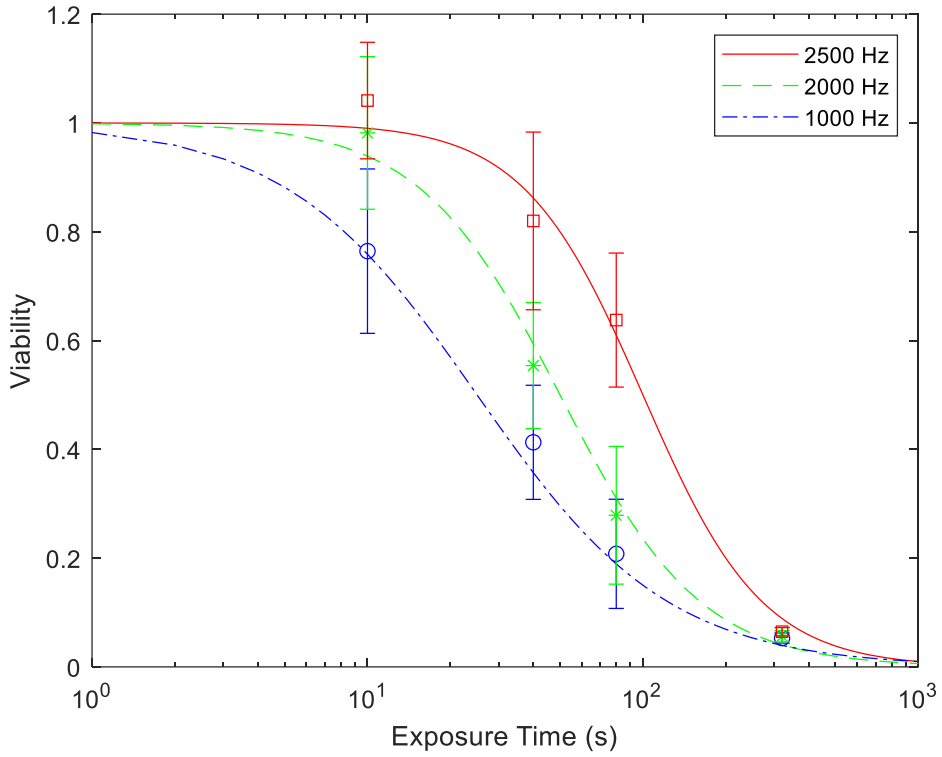

Figure 10: Cytotoxic effects of the pin-to-plate device on U251MG human multiforme glioblastoma cells with different discharge frequencies. All values have been expressed with respect to control, as 100%.

To confirm these findings, U251MG human multiforme glioblastoma cells were exposed to plasma generated at 240 V with the discharge frequency varied from 1000 – 2500 Hz and a duty cycle of 72 μs, with doses of CAP range from 0 s to 320 s. In all cases, a dose dependent cytotoxicity is evident after 96 hours, when measured using the Alamar Blue™ cell

viability assay. In terms of cancer cell line treatment, it can be seen from Figure 10 that the use of a plasma discharge frequency of 1000 Hz has the highest cytotoxic impact. Using a 4-parameter nonlinear logistic equation, the IC_{50} in sodium pyruvate-free media was measured to be ~25 seconds. The observations are consistent with the observations presented in Figure 8, that a discharge frequency of 1000 Hz produced higher quantities of all reactive species measured within the culture medium, and that these generated amounts increased monotonically over the timescale 0 – 320 seconds. The cell viability was tested in 24 wells per plate (centre part of the plate) and replicated 3x, giving a total of 72 wells analysed.

4 Conclusion

The use of human glioblastoma multiform (U-251MG) was to show a potential application of this technology as well as to elucidate the main species required to induce cytotoxicity, and that the treatment is homogenous over large target sample areas. The work demonstrates the potential to perform high throughput screening of samples in wells where co-factors can be introduced. For future clinical applications, the work shows that a scaled down multi-pin discharge in the glow regime could offer a suitable means of treating tissue directly, overcoming the associated challenges of atmospheric air discharges which typically display more filamentous discharges. The optical diagnostics of the large gap atmospheric plasma discharge demonstrated that the discharge frequency plays a vital role in the formation of reactive species. As the frequency was increased, it was found that the optimal discharge frequency was 1000 Hz, as this produced the greatest combination of RNS and ROS within the plasma. However, at higher frequencies, the emission intensities recorded through OES diminished and were not easily detected above 1500 Hz. This was not the case for the detection of O_3, as large levels were still generated even when approaching a discharge frequency of 2500 Hz. This allows for a tailoring of the gas chemistry to produce relatively higher ROS levels over RNS without changing the atmospheric conditions or gas, allowing for dynamic

settings to be used for sample treatments or to highlight which reactive species plays a dominant role for different effects. It has also been shown that, although there were higher emission intensities found around the outer pins of the system a greater density of O_3 was measured in the central region of the system, the area above the placement of the 96-well plate had little variance and allows for a consistent and homogeneous treatment at the sample/plasma boundary. It has been demonstrated that the generation of RNS and ROS in cell culture medium by the plasma is also highly dependent on the plasma discharge frequency, as is the cytotoxicity to glioblastoma cell line. The study demonstrates the importance of appropriate plasma diagnostics and the impact of the plasma generation conditions for potential biomedical applications of this highly promising emerging technology.

Acknowledgements

This work was conducted with the financial support of Science Foundation Ireland (SFI) for authors L.S. and A.C, and also by the TU Dublin Fiosraigh Research Scholarship programme for S.B.

Author Contributions

L.S., P.C., and J.C. conceived the project and designed the experiments. L.S., S.B., A.C., and C.S. performed the experiments, and collected and analysed the data. B.J, R.M., P.C, H.J.B., and J.C. co-wrote the paper. All authors discussed the results and reviewed the manuscript.

Conflict of Interest

Authors Scally and Cullen are, respectively, the plasma engineer and CEO of PlasmaLeap Technologies. PlasmaLeap Technologies supplied the Leap100 system used in this study.

References

[1] R. Thirumdas, C. Sarangapani, and U. S. Annapure, *"Cold Plasma: A Novel Non-Thernal Technology for Food Processing"*, Food Biophysics, Springer, **10**, (2015).

[2] S. Cui, R. Hao, and D. Fu, "*Integrated Method of Non-Thermal Plasma Combined with Catalytical Oxidation for Simultaneous Removal of SO_2 and NO*", Fuel, Elsevier, **246,** (2019).

[3] A. Mahyar, H. Miessner, S. Mueller, K. H. H. Aziz, D. Kalass, D. Moeller, K. Kretschmer, S. R. Manuel, and J. Noack, "*Development and Application of Different Non-Thermal Plasma Reactors for the Removal of Perfluorosurfactants in Water: A Comparitive Study"*, Plasma Chemistry and Plasma Processing, **39** (2019).

[4] G. Nageswaran, L. Jothi, and S. Jagannathan, "*Plasma Assisted Polymer Modifications"*, Non-Thermal Plasma Technology for Polymeric Materials: Applications in Composites, Nanostructured Materials and Biomedical Fields, Chapter 4, 95-127, Elsevier. (2019).

[5] C.-Y. T. Tschang, and M. Thoma, *"Biofilm Inactivation by Synergistic Treatment of Atmospheric Pressure Plasma and Chelating Agents"*, Clinical Plasma Medicine, Elsevier, **15**, (2019).

[6] A. Lin, Y. Gorbanev, J. De Backer, J. Van Loenhout, W. Van Boxem, F, Lemière, P. Cos, S. Dewilde, E. Smits, and A. Bogaerts, *"Non-Thermal Plasma as a Uniqure Delivery System of Short-Lived Reactive Oxygen Species for Immunogenic Cell Death in Melanoma Cells"*, Advances Science, Wiley Online Library, **6**, (2019).

[7] M. S. Moss, K. Yanallah, R. W. K. Allen, and F. Pontiga, *"An Investigation of CO_2 Splitting Using Nanosecond Pulsed Corona Discharge: Effect of Argon Addition on CO_2 Conversion and energy Efficiency"*, Plasma Sources Science and Technology, **26**, (2017).

[8] L. Scally, M. Gulan, L. Weigang, P. J. Cullen, and V. Milosavljevic, *"Significance of a Non-Thermal Plasma Treatment on LDPE Biodegradation with Pseudomonas Aeruginosa"*, MDPI, Materials, **11**, (2018a)

[9] S. Xu, P. I. Khalaf, P. A. Martin, and J. C. Whitehead, *"CO_2 Dissociation in a Packed-Bed Plasma Reactor: Effects of Operating Conditions"*, Plasma Sources Science and Technology, **27**, (2018).

[10] L. Scally, J. Lalor, M. Gulan, P. J. Cullen, and V. Milosavljevic, *"Spectroscopic Study of Excited Molecular Nitrogen Generation Due to Interactions of Metastable Noble Gas Atoms"*, Wiley, Plasma Processes and Polymers, **15**, (2018b).

[11] D. Yan, J. H. Sherman, and M. Keidar, *"Cold Atmospheric Plasma, A Novel Promising Anti-Cancer Treatment Modality"*, NCBI: Oncotarget, **8**, (2017).

[12] A. Dubuc, P. Monsarrat, F. Virard, N. Merbahi, J.-P. Sarrette, S. Laurencin-Dalicieux, and S. Cousty, *"Use of Cold-Atmospheric Plasma in Oncology: A Concise Systemic Review"*, NCBI: Therapeutic Advances in Medical Oncology, **10**, (2018).

[13] D. Yan, W. Xu, X. Yao, L. Lin, J. H. Sherman, and M. Keidar, *"The Cell Activation Phenomena in the Cold Atmospheric Plasma Cancer Treatment"*, Scientific Report, **8**, (2018).

[14] N. Kurake, H. Tanaka, K. Ishikawa, T. Kondo, M. Sekine, K. Nakamura, H. Kajiyama, F. Kikkawa, M. Mizuno, and M. Hori, *"Cell Survival of Glioblastoma Grown in Medium Containing Hydrogen Peroxide and/or Nitrite, or in Plasma-Activated Medium"*, Archives of Biomedical Physics, **605**, (2016).

[15] P. Babington, K. Rajjoub, J. Canady, A. Siu, M. Keidar, and J. H. Sherman, *"Use of Cold Atmospheric Plasma in the Treatment of Cancer"*, AVS: Biointerphases, **10**, (2015).

[16] Z. He, K. Liu, E. Manaloto, A. Casey, G. P. Cribaro, H. J. Byrne, F. Tian, C. Barcia, G. E. Conway, P. J. Cullen, and J. F. Curtin, "*Cold Atmospheric Plasma Induces ATP-Dependent Endocytosis of Nanoparticles and Synergistic U373MG Cancer Cell Death*", Scientific Reports, **8**, (2018).

[17] P. Rajasekaran, P. Mertmann, N. Bibinov, D. Wandke, W. Viöl, and P. Awakowicz, "*Filamentary and Homogeneous Modes of Dielectric Barrier Discharge (DBD) in Air: Investigation through Plasma Characterization and Simulation of Surface Irradiation*", Wiley, Plasma Processes and Polymers, **7**, (2010)).

[18] K. Takaki, M. Shimizu, S. Mukaigawa, and T. Fujiwara, "*Effect of Electrode Shape in Dielectric Barrier Discharge Plasma Reactor for NOx Removal*", IEEE Transaction on Plasma Science, **32**, (2004).

[19] M. J. Johnson, R. Tirumala, and D. B. Go, "*Analysis of Geometric Scaling of Miniature, Multi-Electrode Assisted Corona Discharges for Ionic Wind Generation*", Journal of Electrostatics, **74**, (2015).

[20] C. M. Edelblute, M. A. Malik, and L. C. Heller, "*Antibacterial Efficacy of a Novel Plasma Reactor Without an Applied Gas Flow Against Methicillin Resistant Staphylococcus Aureus on Diverse Surfaces*", Bioelectrochemistry, **112**, (2016).

[21] M. A. Malik and D. Hughes, "*Ozone Synthesis Improves by Increasing Number Density of Plasma Channels and Lower Voltage in a Nonthermal Plasma*", Journal of Physics D: Applied Physics, **49**, (2016).

[22] R. Brandenburg, "*Dielectric Barrier Discharges: Progress on Plasma Sources and on the Understanding of Regimes and Single Filaments*", Plasma Sources, Science, and Technology, **26**, (2017).

[23] L. Zhang, D.-Z. Yang, W.-C. Wang, Z.-J. Liu, S. Wang, P.-C. Jiang, and S. Zhang, "*Atmospheric Air Diffuse Array-Needles Dielectric Barrier Discharge Excited by Positive, Negative, and Bipolar Nanosecond Pulses in Large Electrode Gap*", Journal of Applied Physics, **116**, (2014).

[24] Z.-J. Liu, W.-C. Wang, D.-Z. Yang, S. Zhang, Y. Yang, and K. Tang, "*The Effect of Dielectric Thickness on Diffuse Nanosecond Dielectric Barrier Discharges Using A Needle Array-Plate Electrode Configuration in Air at Atmospheric Pressure*", Journal of Applied Physics, **113**, (2013).

[25] M. A. Naveed, A. Qayyum, S. Ali, and M. Zakaullah, "*Effects of Helium Gas Mixing on the Production of Active Species in Nitrogen Plasma*", Physics Letters A, **5**, (2006).

[26] A. Begum, M. Laroussi, and M. R. Pervez, "*Plasma Jet: Breakdown Process and Propagation Phenomenon*", AIP Advances, **3**, (2013).

[27] P. Lu, D. Boehm, P. Bourke, and P. J. Cullen, "*Achieving Reactive Species Specificity within Plasma Activated Water through Selective Generation using Air Spark and Glow Discharges*", Wiley, Plasma Processes and Polymers, **8**, (2017).

[28] D. Boehm, C. Heslin, P. J. Cullen, and P. Bourke, "*Cytotoxic and Mutagenic Potential of Solutions Exposed to Cold Atmospheric Plasma*", Scientific Reports, **6**, (2016).

[29] S. N. Rampersad, "Multiple Applications of Alamar Blue as an Indicator of Metabolic Function and Cellular Health in Cell Viability Bioassays", MDPI – Sensors, **12**, (2012).

[30] X. T. Deng and M. G. Kong, "*Frequency Range of Stable Dielectric-Barrier Discharges in Atmospheric He and N2*", IEEE Transactions on Plasma Science, **22**, (2004).

[31] C. Sarangapani, M. Danaher, B. Tiwari, P. Lu, P. Bourke, P. J. Cullen, "*Efficacy and Mechanistic Insights into Endocrine Disruptor Degradation using Atmospheric Air Plasma*" Chemical Engineering Journal, **326**, (2017)